Calibration of key temperature-dependent ocean microbial processes in the cGENIE.muffin Earth system model

Katherine A. Crichton[1*], Jamie D. Wilson[2], Andy Ridgwell[3], Paul N. Pearson[1].

[1] School of Earth and Ocean Sciences, Cardiff University, UK
5 [2] BRIDGE, School of Geographical Sciences, University of Bristol, Bristol, UK
[3] Department of Earth Sciences, University of California, Riverside, CA 92521, USA
* now at School of Geography, University of Exeter, EX4 4RJ, UK

Correspondence to: Katherine A. Crichton (k.a.crichton@exeter.ac.uk)

10 **Abstract.** Temperature is a master parameter in the marine carbon cycle, exerting a critical control on the rate of biological transformation of a variety of solid and dissolved reactants and substrates. Although in the construction of numerical models of marine carbon cycling, temperature has been long-recognised as a key parameter in the production and export of organic matter at the ocean surface, it is much less commonly taken into account in the ocean interior. There, bacteria (primarily) transform sinking particulate organic matter into its dissolved constituents and thereby consume dissolved oxygen (and/or other electron acceptors

15 such as sulphate) and release nutrients, which are then available for transport back to the surface. Here we present and calibrate a more complete temperature-dependent representation of marine carbon cycling in the cGENIE.muffin Earth system model, intended for both past and future climate applications. In this, we combine a temperature-dependent remineralisation scheme for sinking organic matter with a biological export production scheme that also includes a temperature-dependent limitation on nutrient uptake in surface waters (and hence phytoplankton growth). Via a parameter ensemble, we jointly calibrate the two parameterisations by

20 statistically contrasting model projected fields of nutrients, oxygen, and the stable carbon isotopic signature (δ^{13}C) of dissolved inorganic carbon in the ocean, with modern observations.

We find that for the present-day, the temperature-dependent version shows as-good-as or better fit to data than the existing tuned non-temperature dependent version of the cGENIE.muffin. The main impact of adding temperature-dependent remineralisation is in driving higher rates of remineralisation in warmer waters and hence a more rapid return of nutrients to the

25 surface there -- stimulating organic matter production. As a result, more organic matter is exported below 80m in mid and low latitude warmer waters as compared to the standard model. Conversely, at higher latitudes, colder water temperature reduces the rate of nutrient supply to the surface as a result of slower in-situ rates of remineralisation.

We also assess the implications of including a more complete set of temperature-dependent parameterisations by analysing a series of historical transient experiments. We find that between the pre-industrial and the present day, in response to a simulated

30 air temperature increase of 0.9°C and ocean warming of 0.12°C (0.6°C in surface waters and 0.02°C in deep waters), a reduction in POC export at 80m of just 0.3% occurs. In contrast, with no assumed temperature-dependent biological processes, global POC export at 80m falls by 2.9% between the pre-industrial and present day as a consequence of ocean stratification and reduced nutrient

supply to the surface. This suggests that increased nutrient recycling in warmer conditions offsets some of the stratification-induced surface nutrient limitation in a warmer world, and that less carbon (and nutrients) then reaches the inner and deep ocean. This

35   extension to the cGENIE.muffin Earth system model provides it with additional capabilities in addressing marine carbon cycling in warmer past and future worlds.

1 Introduction

The cycle of carbon through the ocean is dominated by the production, destruction, and transformation of both dissolved and particulate organic matter (DOM and POM, respectively) (Legendre et al., 2015; Heinze et al., 2015). The 'biological carbon pump'

40   (Fig. 1) is a principal mechanism, operating by removing carbon from the surface and mixed layer waters by phytoplankton photosynthesis and transferring it to the deep by the sinking of organic matter (see: Hülse et al., 2017 for a review). Export out of the near-surface euphotic zone is affected by photosynthesis rates (primary production), but is also affected by grazing, respiration and other food web processes (Steinberg and Landry, 2017; Mari et al., 2017). Of this export, only a fraction reaches the deep ocean through a series of processes involving feeding and remineralisation by microbes and other biota, modulated by sinking speeds and

45   composition of the sinking matter itself (Bach et al., 2016; Rosengard et al., 2015; Turner, 2015). At the ocean floor, organic matter undergoes further microbial degradation and transformation before eventually forming sediments. Removing carbon from surface waters and storing it for centuries (intermediate depths), millennia (deep ocean), or multi-millennia (sediments) controls atmospheric CO_2 levels which would otherwise be much higher (by ~150ppm to 200ppm) in the absence of this biological activity (Parekh et al 2005, Sarmiento and Gruber, 2006). Ocean circulation generally acts against the biological pump, homogenising heterogeneity in

50   the ocean interior and returning carbon (and nutrients) back to the surface. Surface-to-deep gradients and storage of carbon in the ocean is hence a function of the rate of ocean ventilation in conjunction with the rate of biological carbon export and the mean depth at which the organic matter is remineralised.

To a first order, export of carbon out of the mixed layer in a warmer world will be reduced as a consequence of increased ocean stratification reducing nutrient re-supply to surface waters (Portner et al., 2014; Reusch and Boyd, 2013). At the same time,

55   higher water temperatures will increase the metabolic rates of photosynthesising and respiring organisms (Brown et al., 2004). Because respiration is considerably more sensitive to temperature than photosynthesis, this may put further pressure on nutrient demand in surface waters affecting primary production and also, therefore, affecting the rate of carbon export (Boscolo-Galazzo et al 2018). However, the export of carbon and the 'strength' of the biological pump is only one of the pertinent factors in marine carbon cycling. Also important is the 'efficiency' of the biological pump – the fraction of exported carbon that reaches the inner

60   ocean, or alternatively, the mean depth below the surface at which this carbon is remineralised, and dissolved inorganic carbon (DIC) returned to the ocean. A deeper mean remineralisation depth equates to a more 'efficient' biological carbon pump. The sub-surface processes that affect the biological carbon pump efficiency are also temperature-dependent (Bendtsen et al., 2015; Turner 2015; Boscolo-Galazzo et al 2018), complicating the net response of the biological carbon pump and carbon sequestration in the ocean interior to changes in global warming.

65   Until recently, few modelling studies considered sub-surface processes in the ocean carbon cycling response to temperature change (Yamamoto et al., 2018; Cao and Zhang 2017; Laufkotter et al., 2016; Segchneider and Bendtsen, 2013; Chikamoto et al 2012). Hulse et al. (2017) presented an extensive review of how EMICs (Earth System Model of Intermediate Complexity) and box models treat ocean carbon cycle processes and summarised how inner ocean processes are less well constrained than surface processes in many models and how their treatment in models is much more variable. This is also the case for more complex ocean

70   models, such as those participating in CMIP5 (Coupled Model Inter-comparison Project 5) and used to inform the recent IPCC assessment (Burd et al., 2016). Making inner ocean processes temperature-dependent in models has an impact on nutrient distribution and, therefore, on primary production (Tauscher and Oschlies, 2011) as well as biological pump efficiency (Laufkotter et al., 2017).

    In a warmer world, higher ocean temperatures should drive a greater fraction of remineralisation in the upper water column,

75   facilitating increased carbon and nutrient return to the ocean surface. However, higher temperatures will also increase carbon loss at the surface due to lower CO_2 solubility, while at the same time promoting biological carbon uptake. Furthermore, for a geologically rapid and transient warming at the surface such as is currently occurring, increased ocean stratification and hence reduce physical transport will occur. The multiple conflicting influences of temperature mean that even the sign of the feedback between greenhouse warming and ocean carbon cycling is, at the very least, unclear (Yamamoto et al 2018).

80   To help tease apart the varying influences of temperatures on marine carbon cycling and atmospheric CO_2, we present and calibrate a temperature-dependent representation of the biological pump in the current 'muffin' release of the cGENIE EMIC (Earth system Model of Intermediate Complexity) (Cao et al. 2009) (and see statement on 'Code Availability'). Our calibrated configuration is intended for use in global biogeochemical cycling studies that require a fuller consideration of the role of temperature both in the geological past and the future.

85   2 The cGENIE.muffin Earth system model framework

The basic framework of the cGENIE EMIC consists of a 3D frictional-geostrophic approximation ocean circulation model (Edwards and Marsh, 2005), coupled to a 2D dynamic-thermodynamic sea-ice model (Marsh et al., 2011). As per previous calibrations of ocean biogeochemical cycles (e.g. Ridgwell et al., 2007), we employ the ocean circulation and sea-ice model on a 36 x 36 equal area grid (10 degrees of longitude and uniform in the sine of latitude) and couple these with a 2D energy-moisture-balance

90   atmosphere model (Marsh et al., 2011) (an alternative to this – a 3D atmospheric general circulation model (Holden et al., 2016) also exists, but not employed in this study). We employ a commonly-used configuration with 16 vertical levels in the ocean and a present-day bathymetry following Cao et al. (2009). All physics parameters and boundary conditions controlling the climate system follow Cao et al. (2009). The representation of ocean carbon and other biogeochemical cycles together with ocean-atmosphere gas exchange, unless otherwise noted, also follow Cao et al. (2009), and are summarised in more detail below. The temperature-

95   dependent parameterisations that we substitute for the equivalent non temperature-dependent processes in Cao et al. (2009) are described in full in this paper.

It has been suggested that both increased grazing pressure (respiration process) by zooplankton, and primary production by phytoplankton (photosynthesis process), will have an impact on export production in a warmer world (Paul et al., 2015; Turner, 2015). However, in the simplified biologically induced export flux (Maier-Reimer, 1993) scheme (Fig. 2) we apply in cGENIE, we
100 cannot explicitly consider the impact of increased grazing pressure in the surface waters. Rather, we are interested in the wider question of the interaction of (any) temperature-dependent community production (as export production), with temperature-dependent microbial remineralisation in the ocean interior, and its impact on the global ocean carbon cycle.

We apply only the direct effect of temperature on large scale metabolic processes (plankton photosynthesis (growth) and microbial respiration). Other factors such as involving particle size distributions, particle density (Cram et al., 2018) and 'ballasting'
105 (e.g. Wilson et al., 2012), and sinking speed (determined by particle characteristics) (McDonnell et al., 2015), are generally determined within the food web and may be considered to be secondary impacts of temperature dependence as a controller on community structure. In past-climates some of these community structures may have been significantly different. Recently Boyd et al. (2019) defined additional particle pumps in the ocean, involving eddy-subduction, diel vertical migration, mesopelagic migration and seasonal lipid pumps. Including these processes is outside the scope of this study where here we focus on the large-scale effect
110 of temperature on metabolism in the ocean biological carbon pump.

2.1 Standard, non-temperature-dependent model formulation

In the original version of the biological uptake scheme, – 'BIOGEM' (Ridgwell et al., 2007) – nutrients are taken out of the surface ocean layer according to several factors including light incidence, ice fraction, nutrient uptake limitation (Michaelis-Menten type), and a prescribed maximum uptake rate (Eq. 1).
115

$$\Gamma = u_0^{PO_4} \cdot \frac{PO_4}{PO_4 + K^{PO_4}} \cdot (1 - A) \cdot \frac{I}{I_0} \qquad (1)$$

Where:

$u_0^{PO_4}$ maximum uptake rate (mol kg^{-1} yr^{-1})

$\frac{PO_4}{PO_4 + K^{PO_4}}$ nutrient limitation term

120 PO_4 local nutrient concentration (mol kg^{-1})

K^{PO_4} Michaelis Menten half saturation value (mol kg^{-1})

$1 - A$ ice free fraction of sea surface

$\frac{I}{I_0}$ light limitation (based on incidence angle) term

125 Here, the maximum uptake rate, (maximum rate of conversion of dissolved PO_4, phosphate, into organic matter by phytoplankton), has a calibrated value of 9.0×10^{-6} mol kg^{-1} yr^{-1} (Cao et al., 2009), while the calibrated Michaelis Menten half saturation value is 9.0×10^{-7} mol kg^{-1} (Cao et al., 2009).

Nutrient uptake is instantaneously converted into organic matter export (both particulate organic matter (POM) and a fraction as dissolved organic matter (DOM)), and this represents community production (see Fig. 2). This production encompasses

130 the entire surface food web, including the action of primary producers (phytoplankton) and the effect of consumers (e.g. grazers). In this export production model, increases in nutrient uptake are directly transferred to increased production of organic matter that sinks out of the surface layer (at 80m depth). In this single (PO_4) nutrient scheme, dissolved inorganic carbon (DIC) is taken out of solution in the surface layer at a molar ratio of 106:1 to $PO_4$and O_2 at a ratio of - 138:1 with PO_4 (Redfield et al., 1963). POM is partitioned into two fractions, which conceptually are: labile (fraction 1, 'POM1'), and recalcitrant POM (fraction 2, 'POM2')

135 (Ridgwell et al., 2007). POM sinks vertically out of the surface layer and settles with a given velocity (here: 125 m day^{-1}). POM is remineralised throughout the water column using a prescribed remineralisation 'curve' reflecting the decay of POM as it sinks. The prescribed remineralisation 'curve' of relative sinking flux vs. depth (e.g. see: Hülse et al., 2017) is always adhered to (Eq. 2a for POM1, Eq. 2b for POM2). In the sinking curve, the relative flux at each layer (z) is calculated according to an exponential decay function (Ridgwell et al., 2007).

140

$$F_z^{POM1} = F_{z=h_e}^{POM1} . \left((1 - r^{POM}) + r^{POM}. exp\left(\frac{z_{h_e}-z}{l^{POM1}}\right) \right) \tag{2a}$$

$$F_z^{POM2} = F_{z=h_e}^{POM2} . \left((r^{POM}) + r^{POM}. exp\left(\frac{z_{h_e}-z}{l^{POM2}}\right) \right) \tag{2b}$$

Where:

$F_{z=h_e}^{POM}$ POM exported out of the surface layer (at 80m)

145 l^{POM} length-scale (556m for POM1; 1×10^6m for POM2 – effectively infinite and hence no water column decay)

r^{POM} initial proportion of POM into fraction 2 (0.055)

Any POM not remineralised within the water column is instead remineralised at the ocean floor – a 'reflective' boundary condition assumption (see Hulse et al. (2017) for discussion).

150 **2.2 Temperature dependent processes**

In the temperature-dependent version of biological export production, a temperature-dependent growth rate limiter is applied to a characteristic time-scale of ambient nutrient depletion (Eq. 3). A similar scheme but without temperature-dependent remineralisation has previously been applied by Meyer et al. (2016) for PO_4-only uptake, and for 2 nutrients (PO_4 and NO_3) by Monteiro et al. (2012).

$$\Gamma = V_{max} \cdot \frac{PO_4}{PO_4+K^{PO_4}} \cdot (1-A) \cdot \frac{I}{I_0} \cdot \gamma^T \cdot PO_4 \tag{3}$$

155   Where:

γ^T	temperature growth limitation term (see below)
V_{max}	maximum net depletion rate (yr^{-1})
PO_4	local PO$_4$ concentration (mol kg^{-1})
$\dfrac{PO_4}{PO_4+K^{PO_4}}$	nutrient limitation term
K^{PO_4}	Michaelis Menten half saturation value (mol kg^{-1})
$1-A$	ice-free fraction of cell
$\dfrac{I}{I_0}$	light limitation (based on incidence angle) term

Temperature growth limitation is represented by the Arrhenius equation, where T is local temperature (Eq. 4).

165    $$\gamma^T = Ae^{(T/b)} \tag{4}$$

The "Eppley curve" is often applied to model metabolic response to temperature change (Table 1). An improved fitted curve was proposed by Bissinger et al. (2008), with both being based on fitting the model to data from empirical studies. The largest difference between the Bissinger curve and the Eppley curve is the value of *A* (Eq.4). It makes little difference which curve we use because we calibrate V_{max} (Eq.3) which is also a multiplier for the temperature growth limitation term (in Eq. 4). We use the original

170   Eppley et al. (1972) values for *A* and *b* (in Eq. 4) as per Monteiro et al. (2012). Both the Eppley and Bissinger curves gives a Q_{10} value (where Q_{10} is the increase in the rate of the metabolic process with a 10°C increase in temperature) for nutrient uptake as 1.88 (Bissinger et al. 2008).

To calculate the remineralisation rate of POM, an Arrhenius-type equation is applied (as in John et al. 2014) (Eq. 5).

$$k(T) = Ae^{(E_a/RT)} \tag{5}$$

175   Where:

E_a	Activation energy (J mol^{-1})
R	gas constant (J K^{-1} mol^{-1})
T	absolute temperature (K)
A	rate constant as *T* approaches infinity

180

This rate is calculated for local temperature and applied to the local POM flux for each POM fraction individually. For both fractions, sinking rate is 125 m day^{-1}, so for cGENIE's non-uniform ocean depths, the fractional loss of POM due to remineralisation in each layer (*z*) is as Eq. 6.

$$\Delta F_z^{POMn} = k(T)_z^{POMn} . \Delta t(z) \qquad\qquad (6)$$

185

Where n denotes POM fraction (either labile (1) or recalcitrant (2) - distinguished as these have different $k(T)$ values), $\Delta t(z)$ is the time that sinking particles on average spend in layer z.

3 Model tuning methodology

In previous published applications of the cGENIE model, either a temperature dependence in export (e.g. Meyer et al., 2016) OR a
190   temperature dependence in remineralisation (John et al., 2014) have been explored in addressing varying paleo questions. Or more commonly, neither (e.g. Ridgwell and Schmidt, 2010), have been used. Here, we now explore both temperature dependence in export and remineralisation scheme together (Table 2) and as a consequence, it is necessary to jointly re-tune the respective scaling factor in each scheme.

We identify three parameters needing joint re-tuning: 1, The maximum nutrient uptake rate V_{max} (Eq. 3) important for
195   export production. 2, The activation energy, $E_a(1)$ (Eq.5) (the minimum energy required for the transformation of organic carbon into inorganic carbon through respiration processes for the remineralisation of labile POC1, Particulate Organic Carbon type 1) where the labile POC1 dominates that exported from the surface. 3, The fraction of recalcitrant POC2 (denoted as $rPOM$ Eq.2a and Eq.2b, note that in this paragraph values are described for carbon, but apply for nutrient as well) formed at the surface that plays a role in the down-column total POC flux and especially how much of the total POC reaches the very deep ocean.

200   The V_{max} range was chosen by testing the model while retaining the remineralisation version used in John et al. (2014), and selecting a range that gave a reasonable agreement with PO_4 and O_2 concentrations, at 4, 7 and 10. For the initial fraction of POC2, we took the John et al. (2014) version, and applied a testing range that encompassed a range 25-400% around this value ($\times 0.25$, $\times 1.0$, $\times 4.0$). For the $E_a(1)$ (Eq.5) setting, John et al. (2014) used the mid of a range of 50 to 60 kJ/mol for labile POC (range identified in Arndt et al. 2013). We use a lower and higher value of that range, and a selection of values nearer the mean (Table 3). Our
205   ensemble hence consisted of 3 different choices for V_{max}, 3 different choices for initial fraction of POC2, and 6 different choices for $E_a(1)$, for a total of $3\times3\times5 = 45$ different parameter combinations and hence model ensemble member experiments. Values for the two rate constants, A (Eq 5, for POC1 at 9×10^{11} yr^{-1}, for POC2 at 1×10^{14} yr^{-1}) that were calibrated for the modern ocean and the sinking speed of 125 m day^{-1} in John et al. (2014) are retained.

Each of the 45 experiments in the ensemble are spun-up for ten thousand years with pre-industrial boundary conditions:
210   the atmosphere restored to 280 ppm CO_2 and -6.5 ‰ $\delta^{13}CO_2$. Following on from each respective spin-up, each model ensemble member is then forced from year 1700 to 2010 in a transient simulation with atmospheric composition conforming to observed (rising) mean annual trends in CO_2 and (falling) $\delta^{13}CO_2$. This is because global datasets are based on modern (i.e. the past few decades) oceanographic observations, where (especially shallow) distributions of nutrients and oxygen may already have been impacted by historical warming, so model-data comparison with the model pre-industrial steady-state is arguably inappropriate.
215   Direct atmospheric measurements and ice core data has shown that atmospheric $\delta^{13}CO_2$ has dropped with increasing CO_2 due to

fossil fuel emissions (that have a characteristic low δ^{13}C) known as the Suess effect (Keeling, 1979; Rubino et al., 2013). This affects ocean δ^{13}C in a non-uniform manner – affecting (in general) nearer-surface waters more strongly due to ocean physics and circulation patterns.

3.1 Model-data comparison method

220 For the model-data comparison, World Ocean Atlas 2009 (WOA 2009, Levitus et al. 2010) 5° data for phosphate (PO$_4$) and dissolved oxygen (O$_2$) was rescaled to a 10°x10° grid (with a simple linear upscaling) and to the cGENIE model depth scale by averaging over the data depth points that most closely correspond to the cGENIE ocean model depth layer distribution. This depth rescaling produces a global mean depth-uncertainty of 2.2% (of the targeted cGENIE depth). As a result the depth rescaling results in additional small uncertainties of $\pm$ 0.01µmols l^{-1} (at 1 standard deviation) for PO$_4$, and $\pm$ 0.02 µmols l^{-1} for O$_2$. The cGENIE model

225 output from year 2010 of the transient experiments was also rescaled to 10°×10°, and converted to µmols l^{-1} (from mol kg^{-1} using modelled water density) for modelled O$_2$ and PO$_4$, for a direct comparison with the data. In all cases, latitudes higher than 80° were neglected. For PO$_4$, we statistically compare the surface concentration, important for constraining nutrient uptake rates, and the global ocean distribution, which strongly reflects remineralisation and hence the strength and efficiency of the biological pump (plus ocean circulation). For dissolved O$_2$, we statistically compare model and data between 283m to 411m (cGENIE ocean level 4 centred

230 at 346m) as an indication of the dissolved oxygen depletion caused by remineralisation near the bottom of the mixed layer and how well the model can represent this. We also compare the global ocean dissolved oxygen distribution. Given that we are utilizing model-derived temperature distributions in the ocean to project nutrient and oxygen concentrations (plus δ^{13}C distributions) which we then contrast with the respective observed data, we additionally re-grid temperature data (producing an uncertainty of $\pm$0.1°C) in the same way as O$_2$ and PO$_4$ so as to enable us to elucidate biogeochemical biases arising from model-data temperature mismatch.

235 For assessing water column profiles, we defined a set of ocean regions, shown in Figure 3. These regions are similar to those used by Weber et al. (2016), but with some regions reduced in size or separated (Subtropical Pacific limited to South Pacific and North Indian Ocean added). This was done so that within each region ocean water characteristics are broadly similar (including temperature, nutrients, oxygen, salinity) as well as particle fluxes being similar (as Weber et al. 2016). We compare the model distribution of δ^{13}C of DIC with data from Schmittner et al. (2013) by grouping this data into regions (Fig. 3) and creating

240 representative (mean with standard deviation) down-column profiles for δ^{13}C for visual comparison with model outputs in the matching region.

4 Model-data and model-model comparison

4.1 Tuning the temperature-dependent version – model vs. data

We first assess model skill in simulating the temperature distribution in the ocean, given its critical importance in the temperature-

245 dependent calculations of metabolic processes (Fig. 4). We find a generally good model fit to ocean temperature data in mid and low latitudes near-surface waters, and in capturing the first order patterns in benthic temperatures. At high latitudes, cGENIE shows

larger differences as compared with observations, due to deficiencies in modelled ocean circulation and/or surface climate. For instance, the temperature discrepancy throughout the water column in the North Atlantic may be due to an overly-strong AMOC (Atlantic Meridional Overturning Circulation) in the model that delivers too high a volume of warmer surface waters to depth. For

250 the North Pacific, the model underestimation of surface and near-surface temperatures by cGENIE likely reflects insufficient surface stratification and too-deep winter-time mixing of the upper water column.

The simulation results (year 2010 of the transient experiments) are shown in Fig. 5 on Taylor diagrams for their fit to observed distributions of dissolved PO_4 and O_2 in the ocean. Points in Fig. 5 are shaded according to the $E_a(1)$ (Eq.5) value, which has the strongest control on PO_4 and O_2 distribution of the three variables. The overall best-fit to the data for the final CBRU setting

255 was selected as $V_{max} = 10$, $E_a(1) = 54$ kJ mol^{-1}, initial fraction POC2 = 0.008, where the best-fit is determined as the setting with the combined overall lowest RMSE for the PO_4 and O_2 distributions.

Surface nutrients are important in constraining export production. Fig. 6 shows cross-plots for surface PO_4 concentration for the best fit CBRU and the standard model for the selected ocean regions. The addition of temperature dependence in CBRU generally increases the surface nutrient concentration and is in better agreement with data than the standard model. The high surface

260 nutrient regions, Antarctic and the North Pacific, are lower than data in all model cases and this is likely due to the lack of iron limitation in this version of the model, as biological activity removes too much nutrient from the surface waters. In these regions, the temperature-dependent version shows slightly better fit to data than the standard model, as the colder surface water reduces nutrient uptake rates. However, the very lowest nutrient regions (e.g. some south Pacific and some west tropical Atlantic) are slightly higher compared to data for CBRU the temperature dependent version.

265 **4.2 Performance of the temperature-dependent model compared to the standard model**

We contrast the performance of the existing tuned, but non temperature-dependent BIOGEM scheme (CB), with the new tuned temperature dependent scheme (CBRU). Regional water-column profile model outputs for CBRU and CB are plotted against PO_4 from WOA 2009 (Levitus et al. 2010) in Fig. 7. In both schemes, the model was tuned according to its fit to PO_4 and both CBRU and CB show a good fit to data. Some differences can be seen between CBRU and CB in surface mid and low latitude waters, e.g.

270 in the North Indian Ocean and Eastern Tropical Pacific, where nutrients are higher in CBRU in better agreement with data. In higher latitude waters model-data differences may be more related to ocean circulation, as for temperature (Fig. 4), with CB and CBRU very similar in Southern Ocean and North Pacific and CBRU slightly better in the North Atlantic.

We find that the addition of temperature dependent microbial processes generally increases surface nutrient concentrations (as shown in Fig. 8) compared to the standard model (except for the very high southern latitudes). This is especially the case in the

275 low-nutrient gyres with up to 4-times higher PO_4 concentration in CBRU than in CB. In the deeper ocean, nutrient concentration is reduced in the temperature-dependent version except for the North Atlantic (where higher surface nutrients are delivered to the deep via the AMOC) and the high Southern latitudes (with slightly higher PO_4 than the standard model).

The distribution of dissolved oxygen also provides information about the biological pump. Photosynthesis removes CO_2 from ocean waters and adds O_2, where respiration does the opposite. In surface waters and the mixed layer, ventilation with the

280 atmosphere also results in higher oxygen concentration. As a general pattern, respiration progressively reduces dissolved oxygen concentrations down the water column until a minimum is reached. Below that depth – the 'oxygen minimum zone' (OMZ) – ocean circulation reintroduces more oxygenated water masses (ventilated from higher latitude and colder surface waters), slightly increasing dissolved oxygen concentrations again with further depth. In the Antarctic zone (Fig. 9), circulation patterns appear to dominate oxygen content (as CB and CBRU are very similar, but fairly dissimilar to data indicators). The North Pacific region also

285 shows offsets between model and data for O_2, PO_4 and temperature, also suggesting a circulation difference. In low latitude waters CBRU shows a better fit to data between the surface and 500m than CB, suggesting that oxygen depletion rates due to respiration are better described here. Overall, the intensity of the OMZ in both CB and CBRU are in reasonable agreement with data, although in low and mid latitudes warmer waters the OMZ occurs higher in the water column in CBRU than CB.

4.3 Tracing Carbon-13

290 Carbon-13 data are widely used as indicators of ocean circulation and of changes in that circulation over time (Lynch-Stieglitz 2003). Water masses have characteristic carbon-13 signatures, so changes in $\delta^{13}C$ measured at any one location may be at least partially attributed to changes in the water sources. The biological pump also affects the $\delta^{13}C$ of ocean waters. The process of photosynthesis fractionates the carbon that is exchanged (from the dissolved inorganic to the organic form); carbon-12 is preferentially taken up, leaving more carbon-13 in the surface waters (Schmittner et al. 2013). As summarized by Kirtland Turner

295 and Ridgwell (2016), fractionation between POC (and DOC) and $\delta^{13}C$ of $CO_2(aq)$ in cGENIE is a function of the $CO_2(aq)$ concentration and based on an approximation of the model of Rau et al. (1996) (Ridgwell, 2001). This gives rise to a spatial distribution in the $\delta^{13}C$ of exported organic carbon, with lower (more negative values) at higher latitudes, and higher (less negative) value towards the equator, primarily reflecting the temperature control on the concentration of $CO_2(aq)$ in surface waters. The mean flux-weighted $\delta^{13}C$ of POC is around -23‰ for the pre-industrial period, and around -26‰ by the year 2010 due to the Suess effect.

300 As POC is remineralised in the water column, low $\delta^{13}C$ carbon is released into the water, modifying the ambient $\delta^{13}C$ of DIC.

The regional mean and standard deviation of data $\delta^{13}C$, and model CBRU and CB are shown in Fig. 10. For all regions, general patterns are similar to those seen in O_2 concentration, except the Antarctic zone. Benthic and deep water absolute $\delta^{13}C$ values are generally similar to data for both model settings. The model-data offset in mid-depth waters (~800m) in the sub-Antarctic zone may be due to a reduced Antarctic intermediate waters contribution in the model. This may explain similar model-offsets at

305 this depth in the South and East-Tropical Pacific regions. In warm surface waters, $\delta^{13}C$ reduces more quickly with depth in CBRU than CB, as nutrient recycling is occurring faster.

4.4 POC export and implications for biological carbon pump efficiency

The inclusion of a temperature dependence term in remineralisation strongly affects export production via the rate of nutrient recycling, and fundamentally affects the efficiency of the biological carbon pump. To demonstrate the impact of each varied

310 parameter, the export flux of POC (measured at 80m) for every simulation (not only the best-fit CBRU) is shown in Fig. 11. With a lower activation energy requirement (low $E_a(1)$ value), less energy is needed for the remineralisation process to occur, this means

nutrients are returned to surface waters more quickly, production is higher, and so POC flux at 80m is higher. Conversely, the higher the $E_a(1)$ value, the more energy is required to remineralise organic carbon. So, at higher $E_a(1)$, proportionally more organic carbon reaches depth making surface processes less important. The fraction of the POC exported that is recalcitrant and the maximum
315   nutrient uptake rate at the surface becomes less important as $E_a(1)$ increases.

The remineralisation curves for each ocean region is shown in Fig. 12 for the best fit CBRU and CB model for POC (in gC m^{-2} yr^{-1}). CBRU and CB have differing initial POC export fluxes with lower latitude warmer waters showing higher export in CBRU due to the increased nutrient recycling there. A dataset of POC flux (Mouw et al. 2016a) is overlaid on the remineralisation curves (Fig. 12). In both model configurations, the measured Antarctic zone POC flux at shallow and intermediate depths (< 1500m) is
320   significantly lower than in the model. We do not apply iron limitation in the Southern Ocean (or elsewhere), which would limit productivity and POC export, and could explain some of the mismatch at shallower depths. However, the measured flux at depth appears well represented. In deeper waters elsewhere, measured POC flux in warmer regions (e.g. East tropical Pacific, North Indian, East Tropical Atlantic) is generally higher than in the model. This likely reflects additional processes that may increase POC fluxes to depth such as ballasting by minerals (Klaas and Archer, 2002; Wilson et al 2012) and the lower reactivity of POC associated with
325   increased recycling in low latitude plankton ecosystems (Aumont et al., 2017).

Overall, the pattern of the efficiency of the transfer of particles from 80m to 1040m (Fig. 13) in CBRU is similar to that found in Weber et al. (2016), where efficiency of transfer is essentially a measure of the rate of remineralistion; what fraction of the POC exported at 80m reaches 1040m. Colder waters show higher transfer efficiency, with the lowest transfer efficiency seen in the sub-tropical gyres. The CB model has a fixed decay rate for all locations, so the transfer efficiency at any particular depth has a
330   global uniform value.

It should be noted that here we have included all available data from Mouw et al. (2016a) without any attempt to ensure these data are representative of the annual mean (where the model output represents the annual mean). POC flux measurements can be highly dependent on time of year and number of data measurement points available. Some of the model-data mismatch may then be due to a mis-match between the interval in time represented by the data, and the annual mean of the model. For instance, blooms,
335   which are not well represented in the model, may explain some of the very high POC flux values (for example 0.2 gC m^{-2} yr^{-1}) in the North Atlantic and hence why the model annual mean appears to underestimate the flux.

5 Implications of including temperature-dependent microbial processes

This temperature-dependent version of the cGENIE model treats two large scale processes of the biological carbon pump. Firstly, nutrient uptake rates due to the metabolic temperature dependence of photosynthesising marine biota; secondly remineralisation
340   rates of sinking particulate organic matter due to the metabolic temperature dependence of respiring marine biota feeding on that sinking organic matter. The calibrated temperature response of the respiration-based mechanism of remineralisation in the water column is more sensitive to temperature change (a mean $Q10$ of 2.28 over 0°C to 26°C, from Eq.5 using 54 kJ mol^{-1} for $E_a(1)$) than the photosynthesis-based one (the Eppley curve has a $Q10$ of 1.88, in Eq. 3 and 4, Bissinger et al. 2008), in agreement with

fundamental studies (Brown 2004). Historical temperature rise, which we induced in the cGENIE.muffin Earth system model by
345 prescribing the observed CO_2 transient in the atmosphere, provides an illustrative example of the role and importance of including
sufficient temperature-dependent processes in models. In this section we therefore discuss in more detail the transient differences
between CB and CBRU model configurations.

Between the years 1700 and 2010, global mean air temperature in cGENIE increases by 0.94°C. In turn, warming at the
ocean surface induces stratification in the water column, reducing nutrient re-supply to the surface from subsurface waters. In the
350 CB model, this results in a pronounced drop in POC export at 80m (Fig. 14). In CBRU this effect is largely offset by the intensified
recycling of nutrients in warmer surface and near-surface waters. However, the transfer efficiency is affected in CBRU, with a drop
of over 5% in the proportion of POC exported at 80m that reaches 1040m. The largest transfer efficiency drops are seen in low and
mid latitude waters (Fig. 15). This reduction in biological pump transfer efficiency is a result of increased rates of remineralisation
in the warming water column, principally in surface and near-surface waters (while whole (volumetrically-weighted) ocean warming
355 is 0.12°C over this period, 0.6°C occurs on a global mean basis in surface waters, and 0.02°C in deepest waters).

Between simulation pre-industrial and present-day model states, we found a significantly smaller drop in POC flux at 80m
when temperature dependence was included (CBRU) compared to the standard model (CB). Global POC flux at 80m reduces by
0.3% between pre-industrial and present-day in CBRU, but with increases in the Southern Ocean of around 10% and in the tropics
of around 1%, suggesting an increase in NPP (Net Primary Productivity) in the tropics. Kwiatkowski et al. (2017) identified a
360 reduction in NPP with warming in the tropical ocean of 3±1% per degree of warming, based on responses to ENSO (El Nino
Southern Oscillation) which is on face value inconsistent with our simulation of a possible increase in NPP in the tropics. Their
estimate utilised satellite based NPP products from data on chlorophyll and light incidence, and found that in no data-constraint did
NPP increase in the tropics (although the data constraint varied according to the NPP product used). However, Behrenfeld et al.
(2015) noted that a reduction in chlorophyll does not necessarily represent a reduction in productivity, due to photoacclimation. The
365 satellite based NPP products do not account or correct for this effect, so may well underestimate NPP in warming conditions. In an
earlier study, Taucher and Oschlies (2011) found an increased NPP when temperature dependence was included in modelled future
projections. Laufkotter et al. (2017) found that when including a temperature-dependence and oxygen content-dependent
remineralisation, NPP increased on warming due to intensified nutrient recycling in near-surface water. They suggested this was
largely due to an initial positive bias in surface ocean nutrients. In a second set-up they reduced nutrient recycling in surface waters
370 and find little impact on NPP between the temperature sensitive and temperature independent model in a future projection to 2100
CE.

Most of the regional variability in the flux of POC in the deep sea was explained via particle size and the effect of
temperature on remineralisation in a study by Cram et al. (2018), with oxygen concentration providing only a small improvement
(by reducing nutrient recycling in the Eastern Tropical Pacific). Cavan et al (2017) concluded that the large oxygen minimum zone
375 in the Eastern Tropical North Pacific reduces the rate of remineralisation due to the almost complete absence of zooplankton particle
disaggregation within, and provides a negative feedback to warming. Particle size plays a role in sinking speeds, as larger particles
sink faster (generally), and particle size is a factor in export and transfer efficiency (Mouw et al 2016b). The version of cGENIE we

used does not account for particle size and has a fixed sinking speed globally. The lack of particle size variability and oxygen concentration's role in remineralisation may explain some of the increased POC flux at 80m that the model shows since the pre-industrial period in tropical waters. This tropics POC export increase may also be partly due to initial higher nutrient concentrations compared to data, or to the increased remineralisation rates re-supplying nutrients to the surface. In summary, projected and predicted changes in NPP in low-nutrient warm waters are still subject to large uncertainties (Turner et al. 2015, Cross et al. 2015).

There is also still uncertainty as to the causes and even patterns in POC flux differences in different ocean regions (Henson et al., 2012; Marsay et al., 2015; Weber et al., 2016; Cram et al., 2018). We find the patterns of transfer efficiency (Fig. 13) for CBRU are in broad agreement with Marsay et al. (2015) and Weber et al. (2016). This transfer efficiency is not dependent on surface waters NPP patterns or on how much POC is exported at 80m in cGENIE, however, the absolute amount of carbon reaching the deep ocean does depend on NPP and export. On warming since the pre-industrial period we found a reduced POC flux at 80m as well as a reduction in transfer efficiency, combining to produce a reduction in the strength of the biological carbon pump with warming. This further implies an increased carbon pump strength in cooler climates, as per Heinze et al. (2016).

6 Summary

Substituting temperature-dependent organic matter export and remineralisation parameterisations into cGENIE.muffin, changes patterns of nutrient, dissolved oxygen, and carbon-13 distributions in the ocean compared to the standard model. Although both model variants are tuned in some way to observed PO_4 and O_2 distributions, substantive differences between models occur in response to warming since the pre-industrial period. In response to warming, inclusion of temperature-dependence ameliorates stratification-induced surface nutrient limitations by increasing nutrient recycling nearer to the surface. As a corollary, less carbon and nutrients are delivered to the deep. On cooling, the inverse is expected with more nutrients and carbon reaching depth, and a more efficient ocean carbon pump. Hence temperature-dependency of the biological pump may act as a positive feedback on atmospheric CO_2 concentrations and climate change.

7 Model code availability

The specific version used of the cGENIE.muffin model used in this paper is tagged as release v0.9.7, and has been assigned a DOI: 10.5281/zenodo.3559853. The code is hosted on GitHub and can be obtained by cloning:

https://github.com/derpycode/cgenie.muffin

changing the directory to cgenie.muffin and then checking out the specific release:

$ git checkout v0.9.7

Configuration files for the specific experiments presented in the paper can be found in the directory:

genie-userconfigs\MS\crichtonetal.GMD.2019

Details of the experiments, plus the command line needed to run each one, are given in the readme.txt file in that directory. All other configuration files and boundary conditions are provided as part of the release.

A manual, detailing code installation, basic model configuration, plus an extensive series of tutorials covering various aspects of
410   muffin capability, experimental design, and results output and processing, is provided on GitHub. The latex source of the manual, along with pre-built PDF file can be obtained, by cloning:

https://github.com/derpycode/muffindoc

The muffin manual contains instructions for obtaining, installing, and testing the code, plus how to run experiments. Specifically:
415   Section 1.1 (Installation, configuration, basic usage) – Provides a basic over-view of the software environment required for installing and running muffin. Section 1.2.2 – provides a basic over-view of cloning and testing the code.

Section 1.3 – Provides a basic guide to running experiments (also see 1.6 and 1.7).

Section 1.4 – provides a basic introduction to model output (much more detail is given in Section 12).

HOW-TO Chapter – Provides a detailed guide to cloning the code and configuring both an Ubuntu (18.04) and a MacOS software
420   environment, including netCDF library installation, plus running a basic test.

Author contribution

KAC set-up, ran and analysed the model ensemble and data, JDW and AR developed the temperature dependent remineralisation process, all authors wrote the manuscript.

Acknowledgments

425   KAC was supported by Natural Environment Research Council (NERC) grant number NE/N001621/1 to PNP. JDW was supported by the European Research Council as part of the "PALEOGENiE" project (ERC-2013-CoG-617313). AR acknowledges additional support from the National Science Foundation under Grants 1702913 and 1736771.

References

Arndt, S., Jørgensen, B.B., LaRowe, D.E., Middelburg, J.J., Pancost, R.D. and Regnier, P.: Quantifying the degradation of organic
430   matter in marine sediments: a review and synthesis, Earth-Sci. Rev., 123, 53-86, doi: /10.1016/j.earscirev.2013.02.008, 2013

Aumont, O., van Hulten, M., Roy-Barman, M., Dutay, J.-C., Éthé, C., and Gehlen, M.: Variable reactivity of particulate organic matter in a global ocean biogeochemical model, Biogeosciences, 14, 2321–2341, doi:10.5194/bg-14-2321-2017, 2017

Bach, L.T., Boxhammer, T., Larsen, A., Hildebrandt, N., Schulz, K.G. and Riebesell, U.: Influence of plankton community structure on the sinking velocity of marine aggregates, Global Biogeochem. Cy., 30(8), 1145-1165, doi:10.1002/2016GB005372, 2016.

435   Behrenfeld, M.J., O'Malley, R.T., Boss, E.S., Westberry, T.K., Graff, J.R., Halsey, K.H., Milligan, A.J., Siegel, D.A. and Brown, M.B.: Revaluating ocean warming impacts on global phytoplankton, Nat. Clim. Change, 6(3), 323-330, doi: 10.1038/nclimate2838, 2016.

Bendtsen, J., Hilligsøe, K.M., Hansen, J.L. and Richardson, K.: Analysis of remineralisation, lability, temperature sensitivity and structural composition of organic matter from the upper ocean, Prog. Oceanogr., 130, 125-145, doi:
440   10.1016/j.pocean.2014.10.009, 2015.

Bissinger, J.E., Montagnes, D.J., harples, J. and Atkinson, D.: Predicting marine phytoplankton maximum growth rates from temperature: Improving on the Eppley curve using quantile regression, Limnol. Oceanogr., 53(2), 487-493, doi: 10.4319/lo.2008.53.2.0487, 2008.

Boscolo-Galazzo, F., Crichton, K.A., Barker, S. and Pearson, P.N.: Temperature dependency of metabolic rates in the upper ocean:
445   A positive feedback to global climate change?, Global Planet. Change, 170, 201-212, doi: 10.1016/j.gloplacha.2018.08.017, 2018.

Boyd, P.W., Claustre, H., Levy, M., Siegel, D.A. and Weber, T.: Multi-faceted particle pumps drive carbon sequestration in the ocean, Nature, 568, 327-335, doi:10.1038/s41586-019-1098-2, 2019.

Brown, J.H., Gillooly, J.F., Allen, A.P., Savage, V.M. and West, G.B., 2004. Toward a metabolic theory of ecology. Ecology, 85(7),
450   pp.1771-1789.

Burd, A.B., Frey, S., Cabre, A., Ito, T., Levine, N.M., Lønborg, C., Long, M., Mauritz, M., Thomas, R.Q., Stephens, B.M. and Vanwalleghem, T.: Terrestrial and marine perspectives on modeling organic matter degradation pathways. Global change biology, 22, 121-136, doi: 10.1111/gcb.12987, 2016.

Cao, L., Eby, M., Ridgwell, A., Caldeira, K., Archer, D., Ishida, A., Joos, F., Matsumoto, K., Mikolajewicz, U., Mouchet, A., Orr,
455   J.C., Plattner, G.K., Schlitzer, R., Tokos, K., Totterdell, I., Tschumi, T., Yamanaka, Y., Yool, A.: The role of ocean transport in the uptake of anthropogenic CO2, Biogeosciences, 6, 375–390, doi: 10.5194/bg-6-375-2009, 2009.

Cao, L. and Zhang, H.: The role of biological rates in the simulated warming effect on oceanic CO2 uptake, J. Geophys. Res.-Biogeo., 122(5), pp.1098-1106, doi: 10.1002/2016JG003756, 2017.

Cavan, E.L., Trimmer, M., Shelley, F. and Sanders, R.: Remineralization of particulate organic carbon in an ocean oxygen minimum
460   zone, Nature Comms., 8, 14847, doi: 10.1038/ncomms14847, 2017.

Chikamoto, M.O., Abe-Ouchi, A., Oka, A. and Smith, S.L.: Temperature-induced marine export production during glacial period, Geophys. Res. Lett., 39, doi: 10.1029/2012GL053828, 2012.

Cram, J.A., Weber, T., Leung, S.W., McDonnell, A.M., Liang, J.H. and Deutsch, C.: The role of particle size, ballast, temperature, and oxygen in the sinking flux to the deep sea, Global Biogeochem. Cy., 32(5), 858-876, doi: 10.1029/2017GB005710, 2018.

465   Cross, W.F., Hood, J.M., Benstead, J.P., Huryn, A.D. and Nelson, D.: Interactions between temperature and nutrients across levels of ecological organization, Glob. Change Bio., 21(3), 1025-1040, doi: 10.1111/gcb.12809, 2015.

Eppley, R.W.: Temperature and phytoplankton growth in the sea, Fish. bull, 70(4), 1063-1085, 1972.

Edwards, N.R. and Marsh, R.: Uncertainties due to transport-parameter sensitivity in an efficient 3-D ocean-climate model, Clim. Dynam., 24(4), 415-433, doi: 10.1007/s00382-004-0508-8, 2005.

470   Heinze, C., Hoogakker, B.A. and Winguth, A.: Ocean carbon cycling during the past 130,000 years-a pilot study on inverse paleoclimate record modelling, Clim. Past, 12, 1949–1978, doi: 10.5194/cp-12-1949-2016, 2016.

Heinze, C., Meyer, S., Goris, N., Anderson, L., Steinfeldt, R., Chang, N., Le Quéré, C. and Bakker, D.C.: The ocean carbon sink-impacts, vulnerabilities and challenges, Earth Syst. Dynam., 6(1), 327, doi: 10.5194/esd-6-327-2015, 2015.

Henson, S.A., Sanders, R. and Madsen, E.: Global patterns in efficiency of particulate organic carbon export and transfer to the deep

475   ocean, Global Biogeochem. Cy., 26(1), doi: 10.1029/2011GB004099, 2012.

Holden, P.B., Edwards, N.R., Fraedrich, K., Kirk, E., Lunkeit, F. and Zhu, X.: PLASIM–GENIE v1. 0: a new intermediate complexity AOGCM, Geosci. Model Dev., 9, 3347-3361, doi: 10.5194/gmd-9-3347-2016, 2016.

Hülse, D., Arndt, S., Wilson, J.D., Munhoven, G. and Ridgwell, A.: Understanding the causes and consequences of past marine carbon cycling variability through models, Earth-Sci. Rev., 171, 349-382, doi: 10.1016/j.earscirev.2017.06.004, 2017.

480   John, E.H., Wilson, J.D., Pearson, P.N. and Ridgwell, A.: Temperature-dependent remineralization and carbon cycling in the warm Eocene oceans, Palaeogeogr. Palaeocl., 413, 158-166, doi: 10.1016/j.palaeo.2014.05.019, 2014.

Keeling, C.D.: The Suess effect: 13Carbon-14Carbon interrelations, Environ. Int., 2(4-6), 229-300, doi: 10.1016/0160-4120(79)90005-9, 1979.

Kirtland Turner, S. and Ridgwell, A.: Development of a novel empirical framework for interpreting geological carbon isotope

485   excursions, with implications for the rate of carbon injection across the PETM, Earth Planet. Sc. Lett., 435, 1-13., doi: 10.1016/j.epsl.2015.11.027, 2016.

Klaas, C. and Archer, D.E.: Association of sinking organic matter with various types of mineral ballast in the deep sea: Implications for the rain ratio. Global Biogeochem. Cy., 16(4), 63-1-14, doi: 10.1029/2001GB001765, 2002.

Kwiatkowski, L., Bopp, L., Aumont, O., Ciais, P., Cox, P.M., Laufkötter, C., Li, Y. and Séférian, R.: Emergent constraints on

490   projections of declining primary production in the tropical oceans, Nat. Clim. Change, 7(5), 355-358, doi: 10.1038/nclimate3265, 2017.

Laufkötter, C., John, J.G., Stock, C.A. and Dunne, J.P.: Temperature and oxygen dependence of the remineralization of organic matter, Global Biogeochem. Cy., 31(7), 1038-1050, doi: 10.1002/2017GB005643, 2017.

Laufkötter, C., Vogt, M., Gruber, N., Aumont, O., Bopp, L., Doney, S.C., Dunne, J.P., Hauck, J., John, J.G., Lima, I.D. and Seferian,

495   R.: Projected decreases in future marine export production: the role of the carbon flux through the upper ocean ecosystem, Biogeosciences, 13, 4023-4047, doi: 10.5194/bg-13-4023-2016, 2016.

Legendre, L., Rivkin, R.B., Weinbauer, M.G., Guidi, L. and Uitz, J.: The microbial carbon pump concept: Potential biogeochemical significance in the globally changing ocean, Prog. Oceanogr., 134, 432-450, doi: 10.1016/j.pocean.2015.01.008, 2015.

Levitus, S., Locarnini, R.A., Boyer, T.P., Mishonov, A.V., Antonov, J.I., Garcia, H.E., Baranova, O.K., Zweng, M.M., Johnson,

500   D.R. and Seidov, D.: World ocean atlas 2009. National Oceanographic Data Center (U.S.), Ocean Climate Laboratory, United States, National Environmental Satellite, Data, and Information Service, 2010.

Lynch-Stieglitz, J.: Tracers of past ocean circulation, Treatise on geochemistry, 6, 433-451, doi: 10.1016/B0-08-043751-6/06117-X, 2003.

Mari, X., Passow, U., Migon, C., Burd, A.B. and Legendre, L.: Transparent exopolymer particles: Effects on carbon cycling in the
505   ocean, Prog. Oceanogr., 151, 13-37, doi: 10.1016/j.pocean.2016.11.002, 2017.

Marsay, C.M., Sanders, R.J., Henson, S.A., Pabortsava, K., Achterberg, E.P. and Lampitt, R.S.: Attenuation of sinking particulate organic carbon flux through the mesopelagic ocean, P. Natl. Acad. Sci USA, 112(4), 1089-1094, doi: 10.1073/pnas.1415311112, 2015.

Marsh, R., Müller, S.A., Yool, A. and Edwards, N.R.: Incorporation of the C-GOLDSTEIN efficient climate model into the GENIE
510   framework:"eb_go_gs" configurations of GENIE, Geosci. Model Dev., 4, 957-992, doi: 10.5194/gmd-4-957-2011, 2011.

McDonnell, A.M., Boyd, P.W. and Buesseler, K.O.: Effects of sinking velocities and microbial respiration rates on the attenuation of particulate carbon fluxes through the mesopelagic zone. Global Biogeochem. Cy., 29(2), 175-193, doi: 10.1002/2014GB004935, 2015.

Meyer, K.M., Ridgwell, A. and Payne, J.L.: The influence of the biological pump on ocean chemistry: implications for long-term
515   trends in marine redox chemistry, the global carbon cycle, and marine animal ecosystems, Geobiology, 14(3), 207-219, doi: 10.1111/gbi.12176, 2016.

Maier-Reimer, E.: Geochemical cycles in an ocean general circulation model. Preindustrial tracer distributions, Global Biogeochem. Cy., 7(3), 645-677, doi: 10.1029/93GB01355, 1993.

Monteiro, F.M., Pancost, R.D., Ridgwell, A. and Donnadieu, Y.: Nutrients as the dominant control on the spread of anoxia and
520   euxinia across the Cenomanian-Turonian oceanic anoxic event (OAE2): Model-data comparison, Paleoceanography, 27(4), doi: 10.1029/2012PA002351, 2012.

Mouw, C.B., Barnett, A., McKinley, G.A., Gloege, L. and Pilcher, D.: Global ocean particulate organic carbon flux merged with satellite parameters, Earth Syst. Sci. Data., 8(2), 531, doi: 10.5194/essd-8-531-2016, 2016a.

Mouw, C.B., Barnett, A., McKinley, G.A., Gloege, L. and Pilcher, D.: Phytoplankton size impact on export flux in the global ocean.
525   Global Biogeochem. Cy., 30(10), 1542-1562, doi: 10.1002/2015GB005355, 2016b.

Parekh, P., Follows, M.J. and Boyle, E.A.: Decoupling of iron and phosphate in the global ocean, Global Biogeochem. Cy., 19(2), doi: 10.1029/2004GB002280, 2005.

Paul, C., Matthiessen, B. and Sommer, U.: Warming, but not enhanced CO2 concentration, quantitatively and qualitatively affects phytoplankton biomass, Mar. Ecol. Prog. Ser., 528, 39-51, doi: 10.3354/meps11264, 2015.

530 Pörtner, H.O., Karl, D.M., Boyd, P.W., Cheung, W., Lluch-Cota, S.E., Nojiri, Y., Schmidt, D.N., Zavialov, P.O., Alheit, J., Aristegui, J. and Armstrong, C.: Ocean systems. In Climate change 2014: impacts, adaptation, and vulnerability. Part A: global and sectoral aspects. contribution of working group II to the fifth assessment report of the intergovernmental panel on climate change (pp. 411-484). Cambridge University Press. 2014.

Redfield, A.C., 1963. The influence of organisms on the composition of seawater. The Sea, 2, 26-77.

535 Reusch, T.B. and Boyd, P.W.: Experimental evolution meets marine phytoplankton, Evolution, 67(7), 1849-1859, doi: 10.1111/evo.12035, 2013.

Ridgwell, A.J.: Glacial-interglacial perturbations in the global carbon cycle, PhD Thesis University of East Anglia Norwich. 2001.

Ridgwell, A., Hargreaves, J.C., Edwards, N.R., Annan, J.D., Lenton, T.M., Marsh, R., Yool, A. and Watson, A.: Marine geochemical data assimilation in an efficient Earth System Model of global biogeochemical cycling, Biogeosciences, 4(1), 87-104, doi:
540 10.5194/bg-4-87-2007, 2007.

Ridgwell, A. and Schmidt, D.N.: Past constraints on the vulnerability of marine calcifiers to massive carbon dioxide release, Nat. Geosci., 3(3), p.196. doi: 10.1038/ngeo755, 2010.

Rosengard, S.Z., Lam, P.J., Balch, W.M., Auro, M.E., Pike, S., Drapeau, D. and Bowler, B.: Carbon export and transfer to depth across the Southern Ocean Great Calcite Belt. Biogeosciences, 12(13), 3953-3971, doi: 10.5194/bg-12-3953-2015, 2015.

545 Rubino, M., Etheridge, D.M., Trudinger, C.M., Allison, C.E., Battle, M.O., Langenfelds, R.L., Steele, L.P., Curran, M., Bender, M., White, J.W.C. and Jenk, T.M.: A revised 1000 year atmospheric δ13C-CO2 record from Law Dome and South Pole, Antarctica. J. Geophys. Res-Atmos., 118(15), 8482-8499, doi: 10.1002/jgrd.50668, 2013.

Sarmiento, J.L.J.L., Gruber, N.N.: Ocean Biogeochemical Dynamics, 1015 Princeton University Press Princeton, 2006.

Schmittner, A., Gruber, N., Mix, A.C., Key, R.M., Tagliabue, A. and Westberry, T.K.: Biology and air–sea gas exchange controls
550 on the distribution of carbon isotope ratios (δ 13 C) in the ocean, Biogeosciences, 10(9), 5793-5816, doi: 10.5194/bg-10-5793-2013, 2013.

Segschneider, J. and Bendtsen, J.: Temperature-dependent remineralization in a warming ocean increases surface pCO2 through changes in marine ecosystem composition. Global Biogeochem. Cy., 27(4), 1214-1225, doi: 10.1002/2013GB004684, 2013.

Steinberg, D.K. and Landry, M.R.: Zooplankton and the ocean carbon cycle, Annu. Rev. Mar. Sci., 9, 413-444, doi:
555 10.1146/annurev-marine-010814-015924, 2017.

Taucher, J. and Oschlies, A.: Can we predict the direction of marine primary production change under global warming?, Geophys. Res. Lett., 38(2), doi: 10.1029/2010GL045934, 2011.

Turner, J.T.: Zooplankton fecal pellets, marine snow, phytodetritus and the ocean's biological pump. Prog. Oceanogr., 130, 205-248, doi: 10.1016/j.pocean.2014.08.005, 2015.

560 U.S. DOE.: Carbon Cycling and Biosequestration: Report from the March 2008 Workshop, DOE/SC-108, U.S. Department of Energy Office of Science, 81, 2008.

Weber, T., Cram, J.A., Leung, S.W., DeVries, T. and Deutsch, C.: Deep ocean nutrients imply large latitudinal variation in particle transfer efficiency, P. Natl. Acad. Sci USA, 113 (31), 8606-9611, doi: 10.1073/pnas.1604414113, 2016.

Wilson, J.D., Barker, S. and Ridgwell, A.: Assessment of the spatial variability in particulate organic matter and mineral sinking
565 fluxes in the ocean interior: Implications for the ballast hypothesis. Global Biogeochem. Cy., 26(4), doi: 10.1029/2012GB004398, 2012.

Yamamoto, A., Abe-Ouchi, A. and Yamanaka, Y.: Long-term response of oceanic carbon uptake to global warming via physical and biological pumps. Biogeosciences, 15(13), 4163-4180, doi: 10.5194/bg-15-4163-2018, 2018.

570

	Rate constant as T approaches infinity	Multiplier constant for T
	A	*1/b*
Eppley et al. 1972	0.59	0.0633
Bissinger et al. 2008	0.81	0.0631

Table 1, Values for variables in eqn 2

Name	Circulation	Biogeochemistry	1. Temperature-dependent uptake	2. Temperature-dependent remineralisation	Description
CB	x	x			Standard model
CBRU	x	x	x	x	Temperature-dependent model

Table 2, Model settings, processes included in each set-up. Column numbering corresponds to numbering in figure 1.

Variable	Values applied
Vmax	4,7,10
POC fraction 2 (recalcitrant)	0.002, **0.008**, 0.032
Ea1 (labile fraction) x10^3J/mol	53, 54, **55**, 56, 60

575 **Table 3, setting for variables in CBRU (temperature dependent). Values in bold are those used in John et al. 2014.**
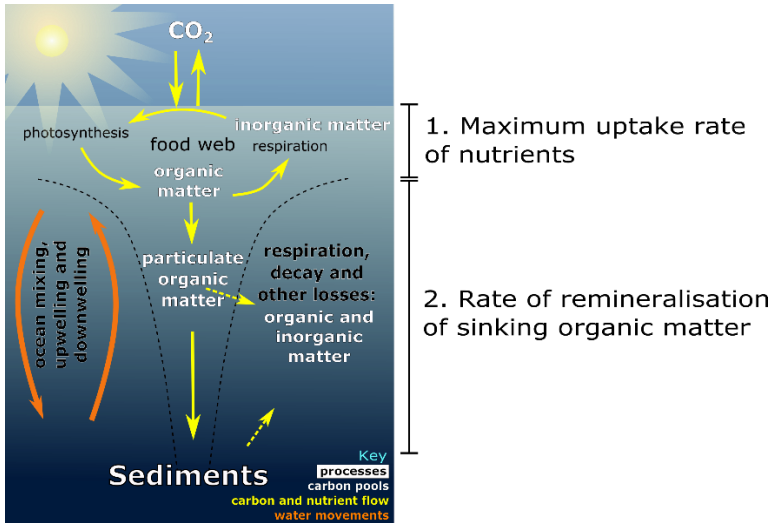
Figure 1, Simplified schematic of the ocean biological pump and dissolved nutrient movements, and the two temperature-dependent processes that are considered in this study 1. Nutrient uptake rates, 2. Remineralisation. In the style of U.S. DOE (2008). We do not model sediments in this study, but it appears in the figure for completeness.

580
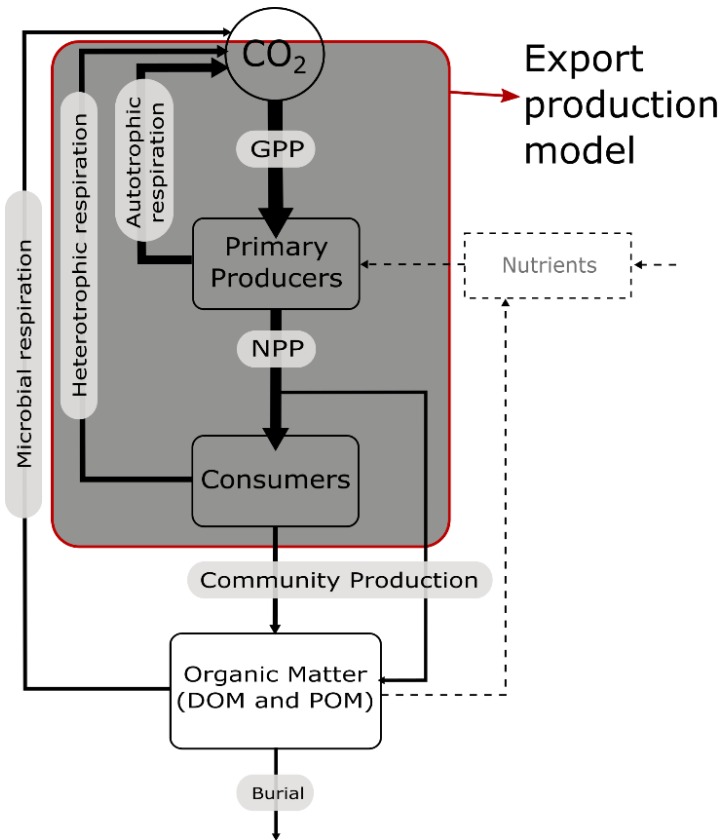
Figure 2. In the export production model, no mechanistic consideration of mixed player plankton respiration vs photosynthesis (GPP) temperature dependence can be considered, but microbial respiration vs community production can be considered, as well as nutrient recycling nearer the surface.

585
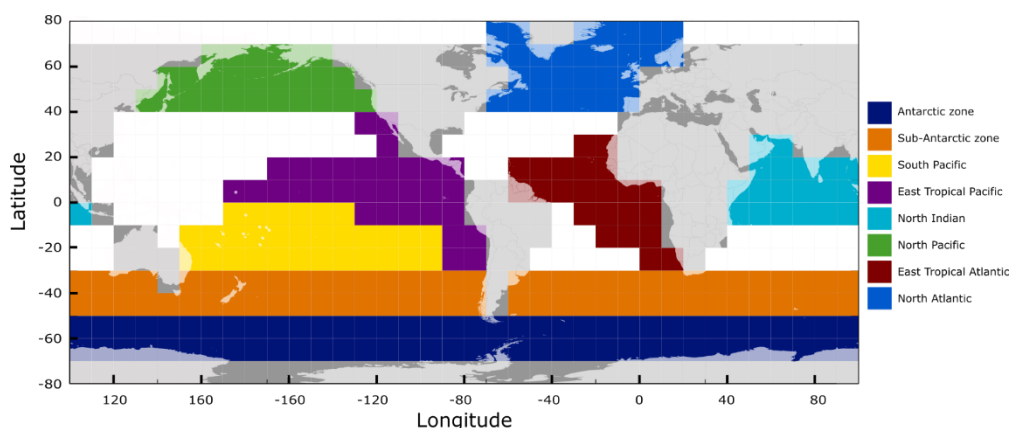
590

Figure 3, Selected ocean regions for model-data comparison (on a 10x10 degree grid, with land masses overlaid for indication), based on Weber et al. (2016) and WOA 2009 data.
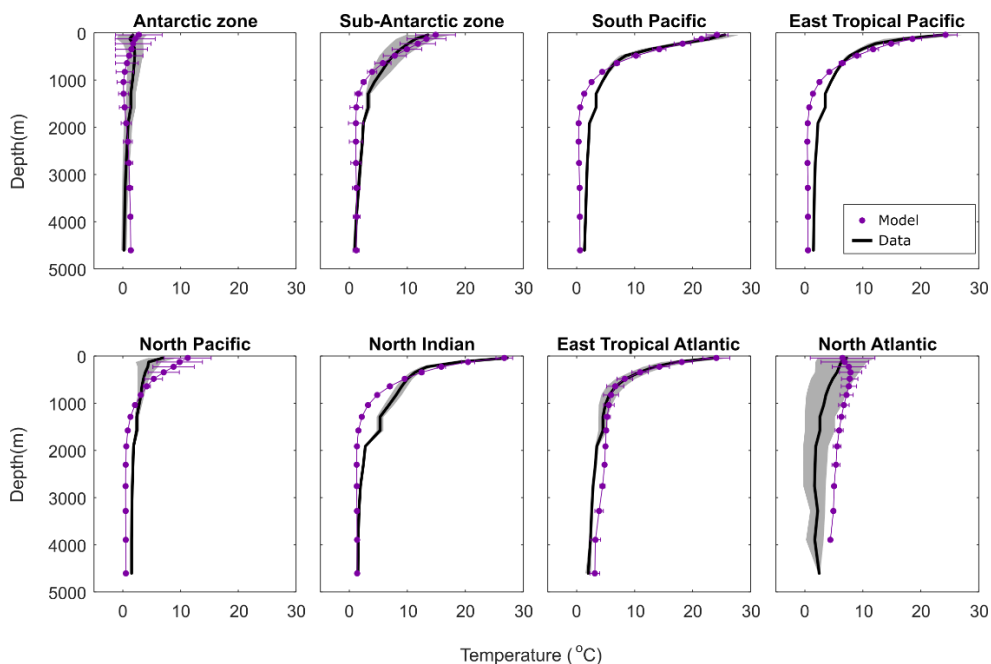
595 **Figure 4, Temperature (°C) per depth by region for model and data (mean and standard deviation). Data WOA 2009 (Levitus et al. 2010).**
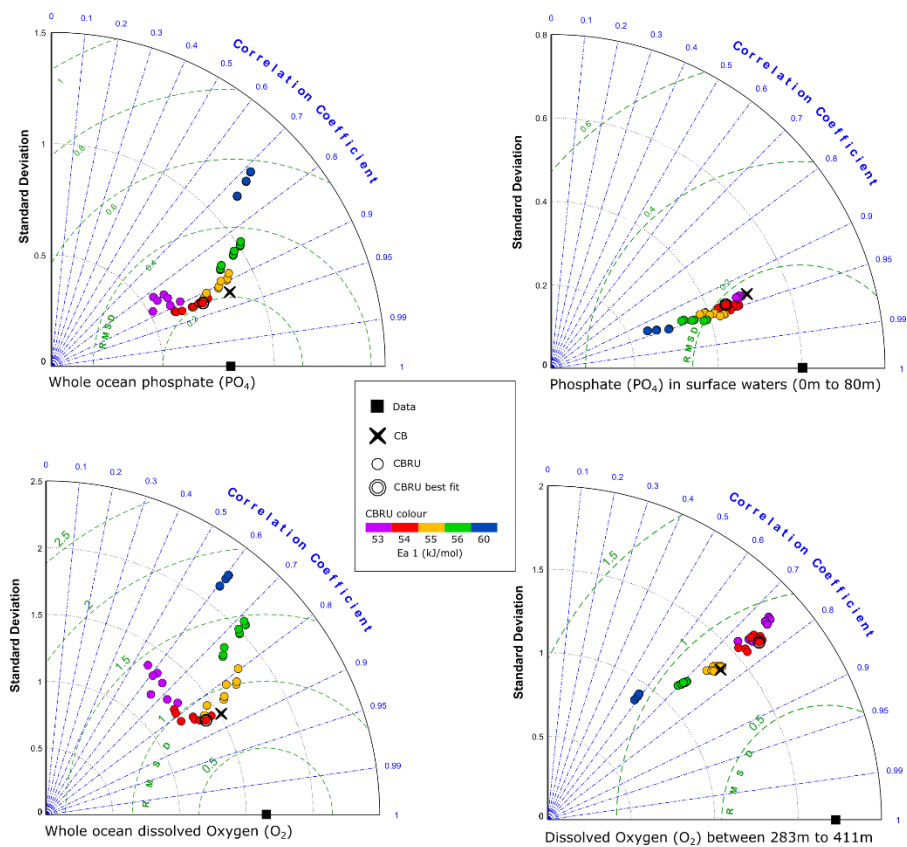
Figure 5, Taylor diagrams for model fit to data for PO4 and O2 concentrations, showing standard deviation (standard deviation is not normalised), correlation and root means squared error (RMSE). Data WOA 2009 (Levitus et al. 2010).
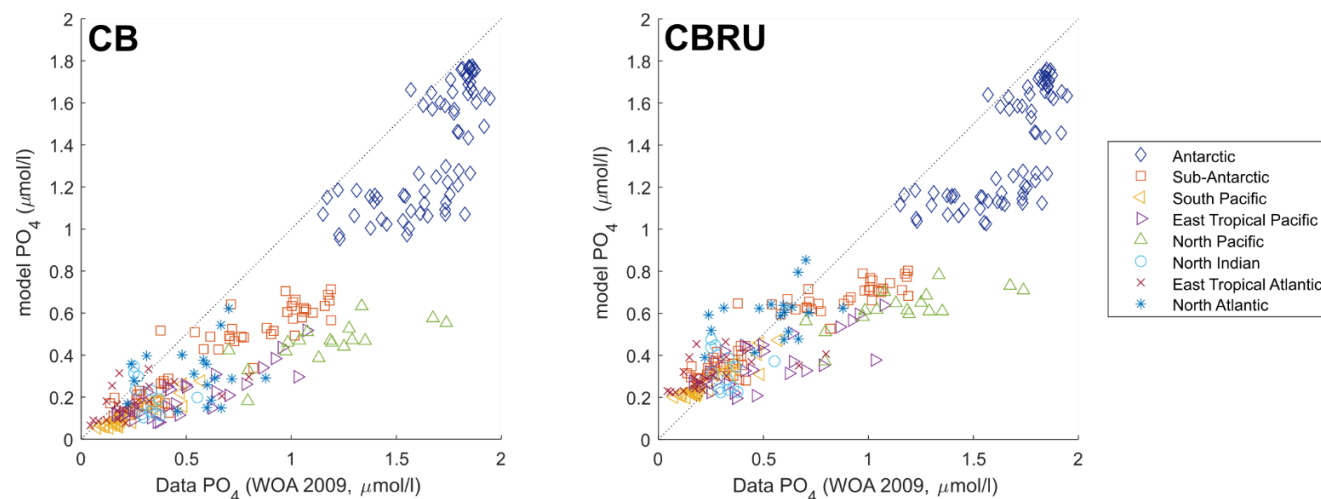
600

Figure 6, Cross plot for surface (0m to 80m) PO₄ concentrations (µmol l⁻¹) for data and model labelled by ocean region. Data WOA 2009 (Levitus et al. 2010)
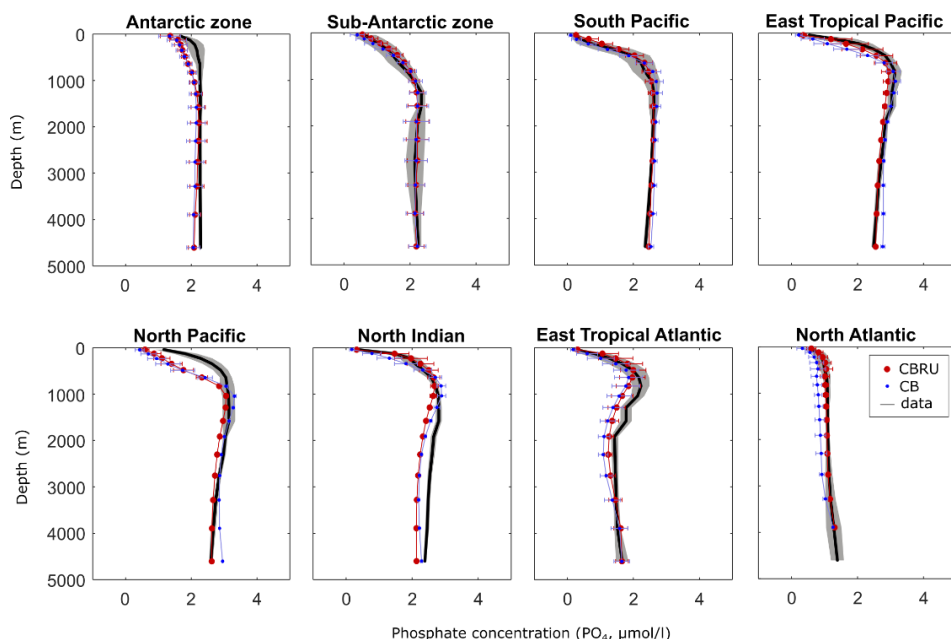
Figure 7, PO₄ (µmol l⁻¹) per depth by region for model and data (mean and standard deviation). Data WOA 2009 (Levitus et al. 2010). CB is standard model, CBRU is temperature dependent model.
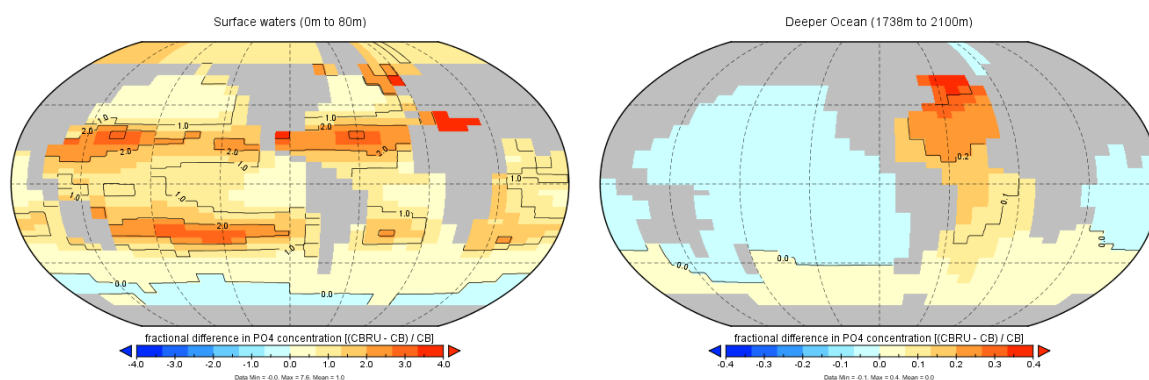
Figure 8, Normalised difference in PO₄ concentration in best-fit CBRU compared to CB (both present-day, note scale difference). CB is standard model, CBRU is temperature dependent model.
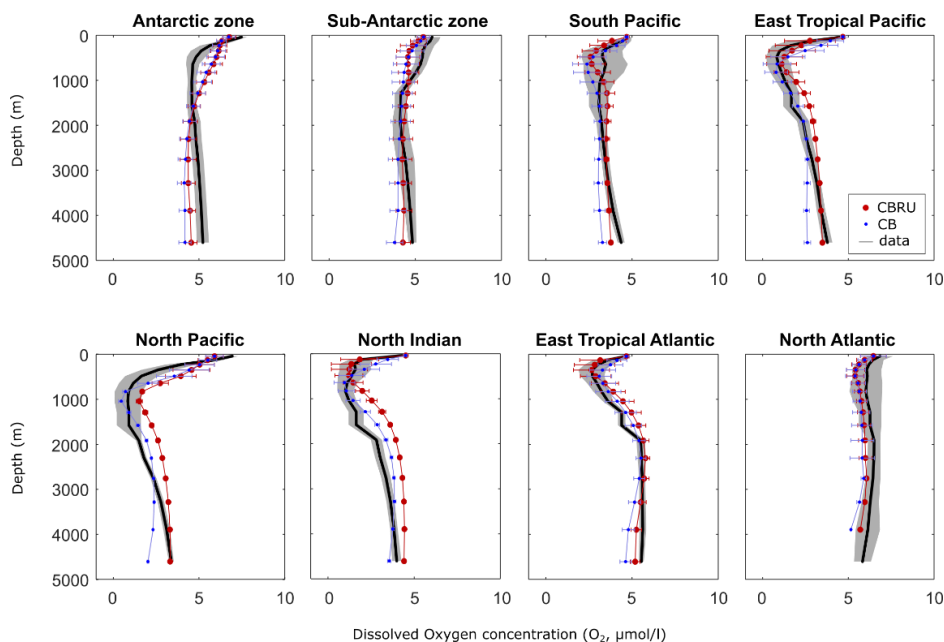
Figure 9, Dissolved O₂ (µmol l⁻¹) per depth by region for model and data (mean and standard deviation). Data WOA 2009 (Levitus et al. 2010). CB is standard model, CBRU is temperature dependent model.
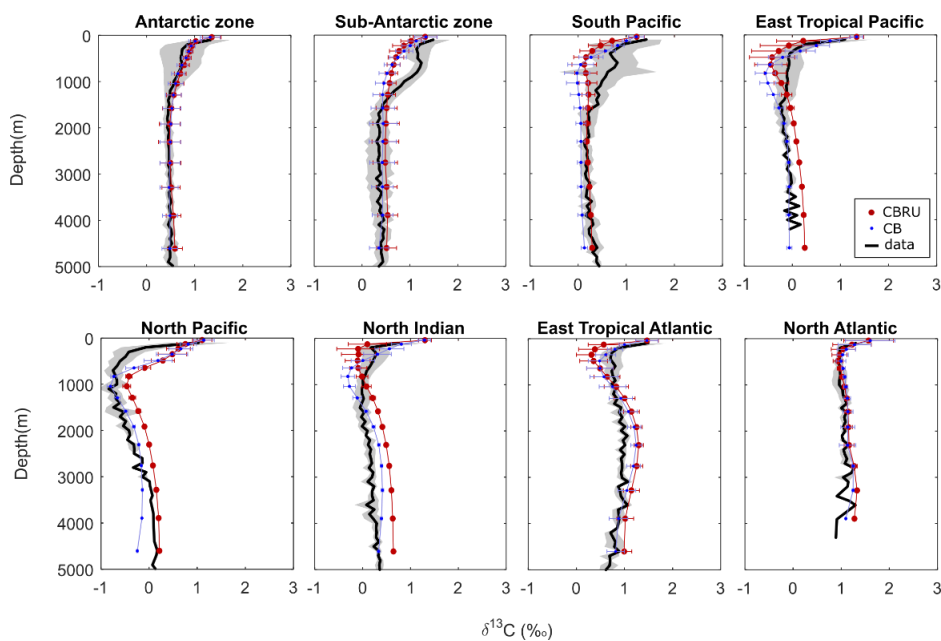
Figure 10, δ¹³C of DIC (‰ VPDB) per depth by region for model and data (mean and standard deviation). Data from Schmittner et al. (2013). CB is standard model, CBRU is temperature dependent model.
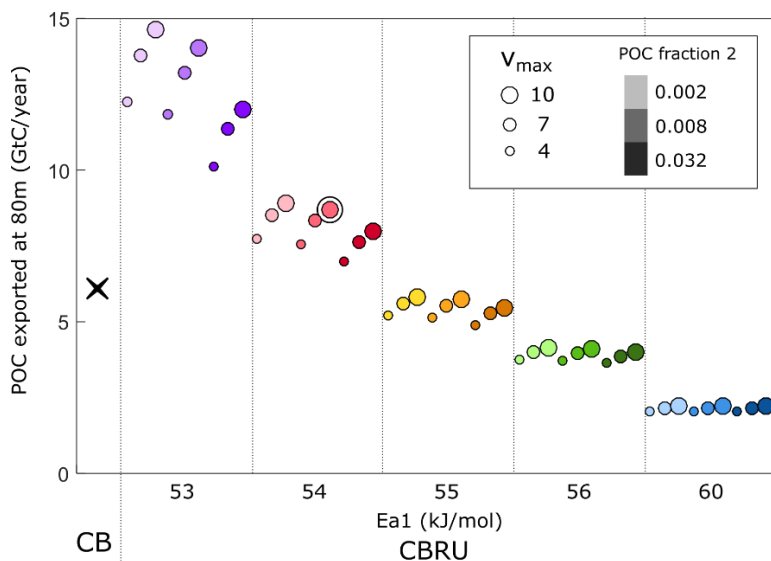
Figure 11, Global POC flux (GtC yr⁻¹) at 80m. Standard model is shown as a black cross, Temperature-dependent model are circles. Best fit CBRU setting double circled. CB is standard model, CBRU is temperature dependent model.
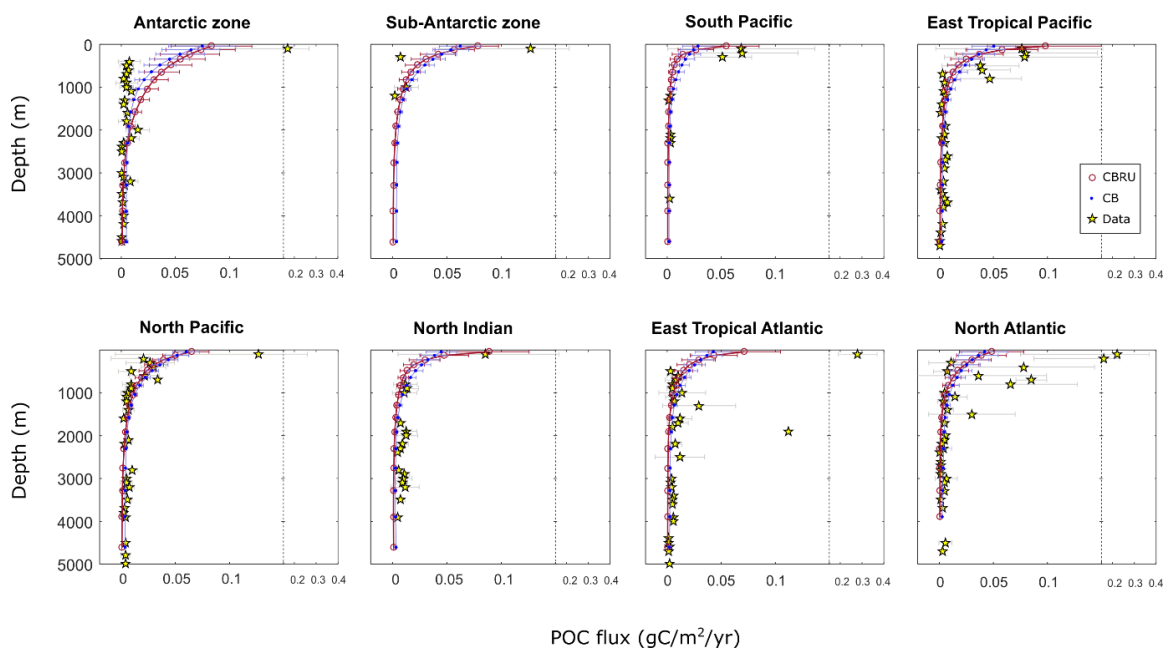
620   **Figure 12, POC flux (gC m⁻² yr⁻¹) for model (mean and standard deviation) and data. Data Mouw et al., 2016a. CB is standard model, CBRU is temperature dependent model.**
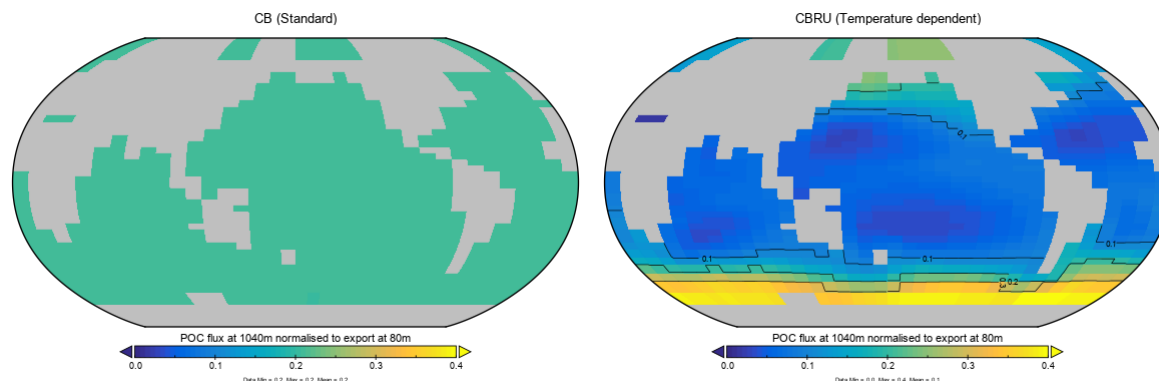
Figure 13, Model POC transfer efficiency (also here used as a measure of biological carbon pump efficiency) for CB (left) and best fit CBRU (right). The fraction of POC exported at 80m that reaches 1040m for the year 2010.
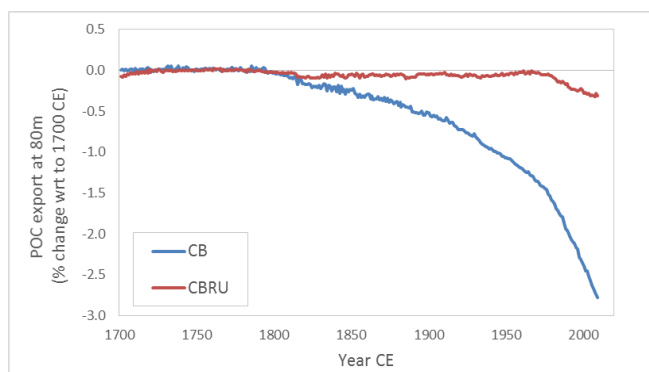
Figure 14, POC export at 80m, % change w.r.t the year 1700. CB is standard model, CBRU is temperature dependent model.
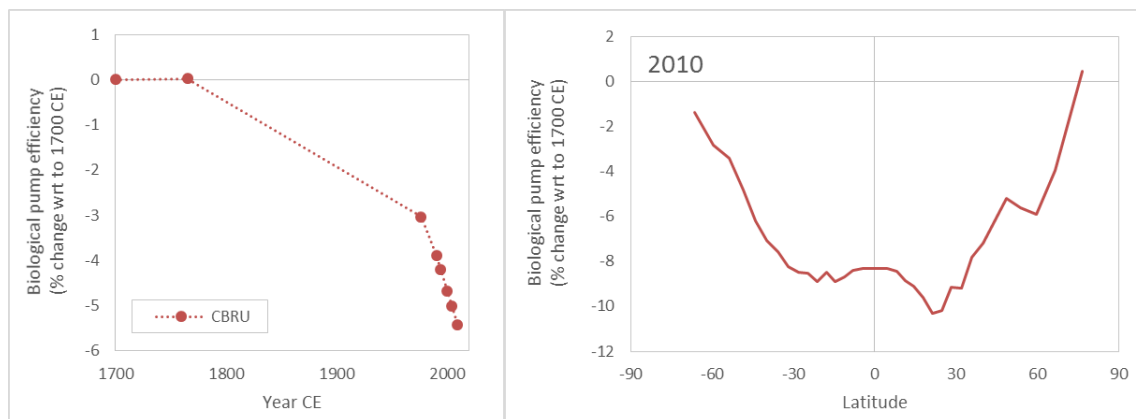
Figure 15, Biological pump "transfer efficiency" (the proportion of POC exported at 80m that reaches 1040m) % change with respect to 1700 CE. Global mean change per year (left) w.r.t 1700; latitudinal change at the year 2010 w.r.t 1700 (right). CBRU is temperature dependent model.